

HYBRID MODEL PREDICTIVE CONTROL TRACKING OF A SAWTOOTH DRIVING PROFILE FOR AN HEV

**Kasemsak
 Uthaichana**
*Caterpillar Inc
 Peoria, IL*

Sorin Bengea
*Eaton Innovation Center
 7945 Wallace Rd, Eden
 Prairie, MN*

Raymond DeCarlo
*Purdue University
 School of ECE
 West Lafayette, IN*

Steve Pekarek
*Purdue University
 School of ECE
 West Lafayette, IN*

Milos Zefran
*University of Illinois
 Dept of ECE
 Chicago, IL*

Abstract—Based on a two-mode operation model of a parallel hybrid electric vehicle (PHEV) developed in previous work, this paper presents a hybrid optimal control solution for the power management problem of a PHEV. The optimal power flows between the vehicle’s main subsystems are computed as solutions of a switching-system optimization (nonlinear programming problem) formulated at the supervisory level assuming a hierarchical vehicle control structure. The resulting equations are numerically solved using collocation methods. The approach is illustrated using the optimal and MPC tracking of a sawtooth velocity driving profile. Unlike other work, the assumption that there is always sufficient power to achieve perfect tracking is not made in this work.

Keywords: hybrid electric vehicles, switching control, hybrid model, supervisory control, power flow, power management

1. INTRODUCTION

Focusing on a PHEV, this paper develops a solution to the *Power Management Control Problem (PMCP)* by determining the power distribution among the main HEV subsystems so that a multi-objective functional is optimized while meeting physical constraints on each HEV subsystem. Within the paradigm of hierarchical control, the PMCP arises naturally at the supervisory level [Rizzoni et al. (1999), Brahma et al. (2000), Lin et al. (2003)]. Using a two-mode HEV switching model [Uthaichana (2006)], the PCMP is formulated as an embedded hybrid optimal control problem (EOCP) [Bengea and DeCarlo (2005)]. The numerical optimization of the embedded PMCP is based on a discretized model via collocation techniques.

2. REVIEW OF A TWO-MODE SWITCHING MODEL FOR PHEV

2.1 Model Hardware Configuration

For this research, the PHEV has two power sources: a conventional ICE and a battery pack-electric drive (ED). The ICE, a four-cylinder, 1.9 L diesel engine, is coupled to the driveshaft through a continuously variable transmission (CVT) (and clutch in the post-transmission configuration [Rahman et al. (2000)]) to facilitate high-efficiency engine operation over a wide range of loads. Coupled to the driveshaft and in parallel with the ICE-CVT, is the ED, a 30 kW, 3-phase, 4-pole induction motor drive operated under maximum torque/amp control [Bodson et al (1995)]. The

ED interfaces with a battery pack consisting of thirty 13 Ah, 12 V, lead acid batteries connected in series. Hotel loads are handled by a traditional engine-based charging system. The ED can operate in unison with the ICE to propel the vehicle or as a generator to charge the battery. Figure 1 illustrates power flows and the main subsystems.

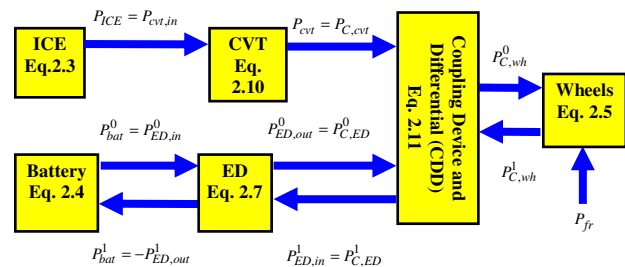


Fig. 1. Power flow diagram with input and output power flow labels.

2.2. Modes of Operation

The blocks and power flows in Figure 1 are used to show that the ED has two modes of operation denoted (using superscripts) as $v = 0$ (motoring) and $v = 1$ (generating). These modes determine the power flow directions. As per [Uthaichana (2006)], a simple parallelism can be made between the two modes of operation considered in this work and the five modes of operations in [Lin et al. (2003)]. Specifically, through careful consideration of the dynamics in each mode of operation, the same modal behavior (i.e., five distinct modes) described in [Lin et al. (2003)] can be captured using only two modes of operation under the supervisory level power flow perspective of this paper. This reduction is a considerable simplification over the mixed power-and-torque based models since PMCP complexity increases exponentially with increased numbers of modes [Nemhauser and Wolsey (1988), Floudas (1995)]. Nevertheless, the two-mode formulation allows an excellent characterization of the PMCP in terms of power flows and velocity/power-dependent efficiencies. Moreover, it makes it possible to solve the PMCP for an HEV by using recent advances in hybrid optimal control theory such as [Bengea and DeCarlo (2005)].

2.3 HEV State Model Overview

Because the ED has faster power flow dynamically than

that of the mechanical subsystems, input-output efficiency dependent algebraic equations suffice at the supervisory level. This leads to the need for only three dynamical states: P_{ICE} (ICE power), \bar{W}_{bat} (normalized battery energy which measures the battery state-of-charge (SOC)), and longitudinal vehicle speed, V , in a mode dependent nonlinear HEV state model:

$$\begin{bmatrix} \dot{P}_{ICE}(t) \\ \dot{\bar{W}}_{bat}(t) \\ \dot{V}(t) \end{bmatrix} = f_v(t) \left(\begin{bmatrix} P_{ICE}(t), \bar{W}_{bat}(t), V(t) \end{bmatrix}^T, u_{v(t)}(t) \right) \quad (2.1)$$

where $f_v(\cdot)$ denotes the motoring, $v = 0$, or generating mode, $v = 1$, equations respectively with controls in mode-0/1 being

$$u_{0/1}(t) = \begin{bmatrix} u_{ICE}(t), u_{FR}(t), u_{EM/GEN}(t) \end{bmatrix}^T \in [0, 1] \times [0, 1] \times [0, 1] \quad (2.2)$$

where $u_{ICE}(t) \in [0, 1]$ is a power command that modulates the maximum available ICE power at a particular engine speed; $u_{FR}(t)$ modulates the maximum allowable frictional vehicle-velocity-dependent braking power, and the power command $u_{EM/GEN}(t) \in [0, 1]$ modulates the rotor speed-dependent maximum available ED power in modes 0 and 1.

This structure is scalable in terms of power sources with only a polynomial increase in optimization complexity [Gill et al. (1981)].

2.3.1 State Equations

The variable $P_{ICE}(t)$ denotes the unidirectional instantaneous ICE power flow to the drivetrain and vehicle through a continuously variable transmission (CVT). The power $P_{ICE}(t)$ is quantified at the flywheel and includes losses due to parasitic loads and is captured by a first order lag differential equation,

$$\dot{P}_{ICE}(t) = -\frac{1}{\tau_{ICE}} P_{ICE}(t) + \frac{1}{\tau_{ICE}} P_{ICE}^{\max}(\omega_{ICE}(V, P_{ICE})) \cdot eng(\omega_{ICE}(V, P_{ICE})) \cdot u_{ICE}(t) \quad (2.3a)$$

where $\tau_{ICE} = 0.3$ s is a nominal engine power delivery delay; the ω_{ICE} -dependent maximum available ICE power is

$$P_{ICE}^{\max}(\omega_{ICE}) = a_1 \left(\frac{\omega_{ICE}}{\max(\omega_{ICE})} \right)^2 + a_2 \left(\frac{\omega_{ICE}}{\max(\omega_{ICE})} \right) + a_3 \quad (2.3b)$$

$\max(\omega_{ICE}) = 3900$, $a_1 = -49.59$, $a_2 = 136.9$, and $a_3 = -14.20$; the CVT controller-selected engine speed is

$$\omega_{ICE} = \omega_{ICE}(V, P_{ICE}) = (1-p)\omega_{ICE}^{\min}(V) + p\omega_{ICE}^{\max}(V) \quad (2.3c)$$

with $p = P_{ICE} / P_{ICE}^{\max}(\omega_{ICE}^{\max}(V))$ and $\omega_{ICE}^{\max}(V)$ and

$\omega_{ICE}^{\min}(V)$ are set forth in [Uthaichana (2006)]; $eng(\omega_{ICE})$ is on (has value 1) or shuts the engine off (has value 0) for

conserving fuel; the resulting control $eng(\omega_{ICE})u_{ICE}(t) \in [0, 1]$ modulates the maximum available engine power, i.e., $P_{ICE}^{\max}(\omega_{ICE}(V, P_{ICE})) \cdot eng(\omega_{ICE}(V, P_{ICE})) \cdot u_{ICE}(t)$ which denotes the desired power flow profile computed and demanded by the supervisory control.

The normalized instantaneous battery energy $\bar{W}_{bat}(t) = W_{bat}(t) / W_{bat}^{\max}$ approximates the battery SOC, defined as the ratio of the instantaneous stored charge to the maximum stored charge where W_{bat}^{\max} is the maximum rated storage energy. This is valid under an assumption of a relatively constant open circuit battery voltage during HEV operation, [Hopka et al. (2000)].

For rendering the EOCP amenable to optimal control methodologies, the model is partially linearized in the battery power control input about the mode-dependent nominal battery operating power, $P_{bat,nom}^v$, resulting in:

$$\dot{\bar{W}}_{bat}(t) = \frac{d_{3,v}}{W_{bat}^{\max}} \left(P_{bat,nom}^v \right)^2 - \left[\ln(d_{1,v} \bar{W}_{bat}(t) + d_{2,v}) + 2d_{3,v} P_{bat,nom}^v + d_{4,v} \right] P_{bat}(t) \quad (2.4)$$

where $P_{bat}(t)$ is the battery power either drawn by (positive for $v = 0$) or provided by the ED (negative for $v = 1$) and is implicitly controlled by $u_{EM/GEN}$. Referring to Figure 1.,

$$P_{bat}(t) = \begin{cases} P_{ED,in}^0(t) & \text{motoring} \\ -P_{ED,out}^1 & \text{generating} \end{cases}$$

The coefficients $d_{k,v}$, $k = 1, \dots, 4$ are chosen to fit the battery efficiency maps making equation 2.4 scalable to a variety of battery storage capacities and types.

The forward-motion differential equation in the vehicle velocity, $V(t)$, is a variation of the standard (torque/force) form to specifically accommodate a power-flow based state model formulation:

$$\dot{V}(t) = -\left(\frac{k_{v1}}{m_c} V^2 + k_{v2} \cos(\alpha(t)) \right) sgn(V(t)) - g \sin(\alpha(t)) + \frac{1000}{m_c (V(t) + \varepsilon_v)} \left[P_{C,wh}^v(t) - P_{FR}(t) \right] \quad (2.5)$$

Here m_c is vehicle mass; $\frac{k_{v1}}{m_c} V^2$ is normalized aerodynamic drag ($k_{v1} = 0.9288$); $k_{v2} \cos(\alpha(t))$ ($k_{v2} = 0.1472$) is the rolling resistance and $\alpha(t)$ denotes the angle of road inclination; $-g \sin(\alpha(t))$ is the gravitational deceleration of the vehicle's longitudinal velocity; $P_{C,wh}^v(t)$ is the coupling device and differential (CDD) power flow to the wheels (positive for propulsion), or power flow from the wheels (negative for regenerative braking); $P_{FR}(t) =$

$P_{FR}^{\max}(V) \cdot u_{FR}(t)$ is the frictional braking power

with $P_{FR}^{\max}(V)$ the velocity-dependent maximum available

braking power, modulated by the normalized control; and ε_V is the regularization term. For practical reasons we choose

$$P_{FR}^{\max}(V) = 50 \tanh(V/5) \quad (2.6)$$

Although equation 2.6 is often expressed in terms of torque [Powell et al. (1998), Waltermann (1996)], our objective is to solve the PMCP. Thus the local control must interpret the frictional braking power of equation 2.6 in terms of rotational wheel speed and torque.

2.3.2 Mode Dependent ED Modeling Equations

As mentioned earlier, the mode-dependent ED model is an algebraic equation:

$$P_{ED,out}^v = \eta_{ED}^v(\omega_{ED}, P_{ED,out}) P_{ED,in}^v \quad (2.7)$$

where $\eta_{ED}^v(\omega_{ED}, P_{ED,out})$ is an efficiency coefficient dependent on the choice of closed-loop control and mode of operation. The choice of the closed loop local control determines the dynamics of the ED and hence the dynamics of the desired input-output power flow map that has been largely ignored in HEV literature. In addition the ED drive rotor speed

$$\omega_{ED} = \omega_{ED}(V) = \lambda_C \cdot k_{v3} \cdot V \quad (2.8)$$

is proportional to the vehicle velocity by a direct lock-up coupling to the wheels through the lower powertrain ($\lambda_C = 1.525$ is a coupling device ratio between the ED shaft speed and the vehicle driveshaft speed, ω_C , and $k_{v3} = 19.26$ is the ratio between the driveshaft and the wheel radius); $P_{ED,out}^v(t)$ denotes the ED mechanical output power when $v = 0$ to help propel the vehicle through the CDD, and when $v = 1$ denotes the ED electrical output power used to charge the battery; (mode $v = 0$, propelling) the controlled ED input power is

$$P_{ED,in}^0(t) = P_{ED,in}^{\max}(\omega_{ED}) \cdot u_{EM}(t) \quad (2.9a)$$

where $u_{EM}(t) \in [0,1]$ modulates the maximum available (rotor speed dependent) power, $P_{ED,in}^{\max}(\omega_{ED})$, under the assumption that there is sufficient battery power in which case, $P_{ED,in}^0(t) = P_{bat}(t) \geq 0$; and ($v = 1$, generating)

$$P_{ED,in}^1(t) = P_{ED,in}^{\max}(\omega_{ED}) \cdot u_{GEN}(t) \quad (2.9b)$$

is the controlled ED mechanical input power delivered through the CDD with $P_{ED,in}^{\max}(\omega_{ED})$ being the speed dependent ED maximum input power modulated by the control $u_{GEN}(t) \in [0,1]$, implying that

$$P_{ED,out}^1(t) = -P_{bat}^1(t) \leq 0.$$

The ED is operated under a maximum torque/amp (MTA) control strategy [Bodson et al. (1995)] since as a local control strategy it is relatively insensitive to machine parameter variation, has relatively fast torque response, and has relatively high efficiencies over the majority of the speed range. [Wasynczuk et al. (1998)] The desired power level

$P_{ED,out}^v$ computed by the supervisor is transformed into an ED torque command, T_E^* , using the rotor speed $\omega_{ED}(V)$.

2.3.3 The CVT

A CVT has the potential to allow the ICE to operate at more fuel efficient engine speeds for a given power command by (instantaneously) choosing the proper gear ratio [Setlur et al. (2003), Foley et al. (2001)]. At the supervisory level, we assume no power response lag between the input and output CVT powers leading to the algebraic equation

$$P_{cvt}(t) = \eta_{cvt} P_{cvt,in}(t) \quad (2.10)$$

where $\eta_{CVT} = 0.95$ is an average efficiency, the input power $P_{cvt,in}(t) = P_{ICE}(t)$, and the output power is delivered to the coupling-device-differential, i.e., $P_{cvt}(t) = P_{C,cvt}(t)$.

2.3.4 Mode-dependent CDD Power Flow Equations

The CDD channels power flows from the ICE-CVT, from or to the ED, and from or to the wheels depending on the mode of operation and whether or not there is regenerative braking. In both modes, we assume that the CDD's power transfer occurs instantaneously and can be modeled as an algebraic equation via conservation of power in terms of the CDD's input/output power flows and efficiencies/losses as:

$$P_{C,wh}^0(t) = \eta_{cdd1} P_{C,cvt} + \eta_{cdd2} P_{C,ED}^0 \quad (2.11a)$$

and

$$P_{C,ED}^1(t) = \eta_{cdd2} P_{C,cvt}(t) - \eta_{cdd2} P_{C,wh}^1(t) \quad (2.11b)$$

where: (i) in both modes, $P_{C,cvt}(t) = P_{cvt}(t) \geq 0$, the CVT output power flow is (without loss) coupled to the input of the CDD; (ii) $\eta_{cdd1} = 1$ is the power transfer efficiency between the CVT output and the wheels; $\eta_{cdd2} = 0.93$ is the power transfer efficiency between the ED and the CVT/wheels; (iii) $P_{C,ED}^0 = P_{ED,out}^0$ is the propulsion power coming directly from the output of the ED in mode-0; in mode-1 $P_{C,ED}^1 = P_{ED,in}^1$ is an output power port of the CDD providing mechanical power to the input of the ED operating as a generator; (iv) the power flow at the wheel-side driveshaft of the CDD in mode-0 is always propulsive, i.e., $P_{C,wh}^0(t) \geq 0$. However, in mode-1, the ICE could provide propulsion power to the wheels, $P_{C,wh}^1(t) \geq 0$, and to the ED, i.e., $P_{C,ED}^1(t) > 0$ simultaneously and $P_{C,wh}^1(t) < 0$ for regenerative braking where the ICE-CVT may also help charge the battery pack i.e., $P_{C,cvt}(t) \geq 0$.

3. THE PCMP AS A SOLUTION OF THE EOCP

3.1. The Idea of the EOCP

This section formulates the PCMP as an EOCP [Bengea

and DeCarlo (2005), Uthaichana et al. (2005)] wherein the modal switching function $v(t)$ takes values not in the set $\{0,1\}$ (the so-called switched optimal control problem (SOCP)), but rather in the closed interval $[0,1]$, i.e., the EOCP. In other words, the original problem of having two distinct modes of operation (SOCP) is embedded into a larger family parameterized by an enlarged mode-switching input $v(t) \in [0,1]$, a continuum of potential values. This embedding converts a non-convex SOCP into a convex EOCP. As per [Bengea and DeCarlo (2005)] the SOCP can almost always be solved by first solving the EOCP and any solution of the EOCP can be approximated to any degree of precision by some solution of the SOCP.

3.2 Formulation of the EOCP

The embedding requires creating a convex combination of the vector fields of equation 2.1:

$$\begin{aligned} \dot{x}(t) &= f_E(x(t), u_0(t), u_1(t), v(t)) \\ &= [1-v(t)]f_0(x(t), u_0(t)) + v(t)f_1(x(t), u_1(t)) \end{aligned} \quad (3.1)$$

Similarly, the performance index (PI) of the EOCP is a convex combination of the PIs associated with each mode of operation of the SOCP:

$$\begin{aligned} J_E(x_0, u_0, u_1, v, [t_0, t_f]) &= g(t_0, x_0, t_f, x_f) \\ &\quad + \int_{t_0}^{t_f} L_E(t, x, u_0, u_1, v) dt \\ &= g(t_0, x_0, t_f, x_f) \\ &\quad + \int_{t_0}^{t_f} [(1-v(t))L_0(t, x, u_0, v) + v(t)L_1(t, x, u_1, v)] dt \end{aligned} \quad (3.2)$$

with $L_0(\cdot)$ and $L_1(\cdot)$ defining the integrands of the PI in modes 0 and 1 respectively. Thus the EOCP (the structure for solving the PMCP) becomes:

$$\text{Min}_{u_0, u_1, v} J_E(x_0, u_0, u_1, v, [t_0, t_f]) \quad (3.3a)$$

with $J_E(\cdot)$ given by equation 3.2, subject to

$$\dot{x}(t) = f_E(x(t), u_0(t), u_1(t), v(t)) \quad (3.3b)$$

with f_E given in equation. 3.1, $v(t) \in [0,1]$, and $u_0, u_1 \in \Omega$ (a compact set).

It can be shown (Corollary 2 in Bengea and DeCarlo (2005)) that the trajectories of the switched system (equation 2.1) are dense in the trajectories of the embedded system (equations 3.3b). If the EOCP has a bang-bang type solution ($v(t)$ only takes values in $\{0,1\}$) then clearly it is also a solution to the original SOCP. These expected relationships between SOCP and EOCP motivate and justify the effort on determining SOCP solutions by solving the EOCP. Additional relationships between the SOCP and EOCP can be found in [Bengea and DeCarlo (2005)].

3.3 Performance Index for PMCP

The choice for the integrand $L_E(t, x, u_0, u_1, v)$ depends on the optimization objective, such as minimizing fuel consumption as in [Anatone et al. (2005), Diop et al. (2002)], or a combination of fuel consumption and emissions as in

[Koot et al. (2005), Lin et al. (2003)], or equivalent fuel consumption [Pisu and Rizzoni (2007)]. For the work reported here, an integral quadratic PI uses the same integrand for both modes of operation, $L_E = L_0 = L_1$:

$$\begin{aligned} J_E &= C_{bat} (\bar{W}_{bat}(t_f) - 0.6)^2 + \int_{t_0}^{t_f} \left(C_V (V(t) - V^{des}(t))^2 \right. \\ &\quad \left. + C_{ICE} \left(\frac{P_{ICE}(t)}{\eta_{ICE}(P_{ICE}, V)} \right)^2 + C_{FR} (P_{FR}(t))^2 \right) dt \end{aligned} \quad (3.4)$$

This PI was selected to explore a tradeoff among velocity

tracking error, $C_V (V(t) - V^{des}(t))^2$, fuel consumption

approximated by ICE power usage divided by fuel

conversion efficiency, $C_{ICE} \left(\frac{P_{ICE}(t)}{\eta_{ICE}(P_{ICE}, V)} \right)^2$, frictional

losses, $C_{FR} (P_{FR}(t))^2$, and the deviation of SOC from the

nominal of 60% at t_f , $C_{bat} (\bar{W}_{bat}(t_f) - 0.6)^2$. This strategy

is similar to the charge-sustaining operation of [Paganelli et al. (2001), Won et al. (2005)]. A more elaborate PI accounting for drivetrain losses can be found in [Uthaichana (2006)].

4. THEORETICAL FOUNDATIONS

The presence of the discrete-valued input $v \in \{0,1\}$ renders, in general, the SOCP non-convex. For a variety of assumptions on system vector fields f_v , cost J_E , and mode-switching penalties and constraints, several approaches have been employed in the literature for characterizing and computing SOCP solutions, consisting of: mode sequences, switching instants, and continuous control values. Without discussing sufficient conditions for optimality nor accounting for the singular solution scenarios [Riedinger et al. (1999)] directly applies the Maximum Principle to the SOCP. For a larger class of systems, and with a cost that depends on the mode sequence, [Sussmann (1999)] derives necessary conditions for optimality via a generalized Maximum Principle. Other approaches include pre-assigned switching sequence method (for a limited class of problems) in [Giua et al. (2001)], and a hybrid Bellman inequality approach in [Hedlund and Rantzer (1999)]. Mixed integer programming (MIP) approaches have also been employed to find optimal solutions [Bemporad and Morari (1999)]. Solving the the SOCP using MIP methods, however, is NP-hard; indeed the scalability of this technique is problematic [Wei et al. (2006)].

The nonconvexity of the SOCP and the inapplicability of the mentioned existing techniques—too general and impractical, or very specific results, or insufficient characterization of the solution—to the SOCP has led to the development the parameterized family of problems, the

EOCP, set forth in the previous section.

4.1 EOCP: Sufficient Existence Conditions

This section summarizes the main sufficient conditions for EOCP's solutions. Sufficient conditions for optimality are [Theorem 9, in Bengea and DeCarlo (2005)]:

- (i) the admissible pair set (control, trajectory) is nonempty;
- (ii) the points $(t, x(t))$ are included in a compact set for all $t \in [t_0, t_f]$;
- (iii) the terminal set is compact;
- (iv) the input constraint set is compact and convex;
- (v) the vector fields f_0 and f_1 are linear in their (control) inputs u_0 , and u_1 , respectively i.e.,

$$(S1) \quad f_0(t, x, u_0) = A_0(t, x) + B_0(t, x)u_0$$

$$(S2) \quad f_1(t, x, u_1) = A_1(t, x) + B_1(t, x)u_1$$

- (vi) for each $(t, x(t))$, the integrands of the penalty functions, $L_0(t, x, u_0)$ and $L_1(t, x, u_1)$, are convex functions of u_0 , and u_1 , respectively.

Based on the assumptions made on the input constraint set and on the vector fields f_0 and f_1 , one can conclude that conditions (i), (ii), and (iv) are met. Further, a sufficiently large compact set can be substituted for the terminal set, meeting condition (iii). Condition (v) is also met by construction (Sections 2) since only the power terms P_{ICE}^{des} , $P_{ED,out}^v$, and P_{FR} depend on the continuous control inputs, and can be factored as a product of two terms, one a control and the other only state dependent $x = [P_{ICE} \quad \bar{W}_{bat} \quad V]^T$. Utilizing again the form of these power terms, and the forms of $L_0(t, x, u_0)$ and $L_1(t, x, u_1)$ one concludes that condition (vi) is also met. Hence the EOCP has a solution.

The above sufficient conditions only guarantee the existence of EOCP's solutions, but do not provide a solution methodology. In conjunction with the SOCP-EOCP relationships mentioned earlier, the necessary conditions obtained by direct application of the Maximum Principle [Uthaichana et al. (2005)] provide a method for obtaining at least suboptimal solutions of the SOCP. By using this approach, the optimization problem is transformed into a two-point boundary value problem on the state and adjoint (co-state) equations where only the initial condition on the state dynamics and the final condition on the adjoint equations are known. However, numerical experimentations with shooting methods for deriving the boundary value problem solutions have demonstrated in [Uthaichana et al. (2005)] that the solution is very sensitive with respect to co-state initial condition. This paper takes the alternate approach of computing numerical solutions for the EOCP via collocation methods, described in the next section.

5. NUMERICAL SOLUTION TECHNIQUE, AND MPC

This section overviews the numerical solution algorithm and the model predictive control (MPC) [Camacho and Bordons (2004)] strategy used in the solution of the PMCP as a solution of the EOCP that underlie the simulation results of the next section. Specifically we discuss the collocation method for solving the HOC problems. [Gregory and Lin (1992), Neuman and Sen (1973), Pytlak and Vinter (1995), Zefran (1996)]

5.1 Discretization via the Collocation Technique

Given the PI of equation 3.2 and the state equation and constraints of equations 3.1, one discretizes these equations using the collocation method. The discretization of the PI uses a variation of the trapezoidal rule to evaluate the integral whereas the state and constraint equations use the mid-point rule. These discretized equations convert the EOCP into a finite dimensional nonlinear programming problem (NLP) where states and inputs are treated as unknown variables. The NLP is solvable using a sequential quadratic programming subroutine, such as *fmincon* in the optimization toolbox of MATLAB. The discretization-and-collocation technique consists of several steps that have two main stages: (i) time discretization, and state and input function approximations by a finite number of polynomial basis functions; (ii) approximation of the continuous state dynamics and cost index integrand by discrete-state and discrete-input-dependent counterparts.

Without going through a lengthy derivation, the continuous time interval $[t_0, t_f]$ is discretized into a sequence of points $t_0 < t_1 < t_2 < \dots < t_{N-1} < t_N = t_f$ where, for simplicity, we take $t_j - t_{j-1} = h$, for $j = 1, \dots, N$. The collocation points are the mid-points, say \hat{t}_j , of the time partitions. A "hat" notation is also used to distinguish the numerically estimated state and control values from their actual counterparts that are "hatless": $\hat{x}_j = \hat{x}(t_j)$,

$$\hat{u}_{0,j} = \hat{u}_0(t_j), \quad \hat{u}_{1,j} = \hat{u}_1(t_j) \quad \text{and} \quad \hat{v}_j = \hat{v}(t_j).$$

The collocation method used here assumes triangular basis functions for the state and piecewise constant basis functions (derivatives of triangular functions) for the controls. The essence of the midpoint rule is to enforce the constraints at the midpoints of each interval $[t_{j-1}, t_j]$ for $j = 1, \dots, N$.

Applying this approach to equation 3.1 results in the discretized embedded state dynamics

$$\begin{aligned} \hat{x}_j = & \hat{x}_{j-1} + h \cdot (1 - \hat{v}_j) \cdot f_0 \left(\frac{\hat{x}_{j-1} + \hat{x}_j}{2}, \hat{u}_{0j} \right) \\ & + h \cdot \hat{v}_j \cdot f_1 \left(\frac{\hat{x}_{j-1} + \hat{x}_j}{2}, \hat{u}_{1j} \right) \end{aligned} \quad (5.1)$$

for $j = 1, \dots, N$, with $f_0(\cdot)$ and $f_1(\cdot)$ the discretized state dynamics. Thus the NLP is to minimize

$$\hat{J} = C_{bat} \left(\hat{W}_{bat,N} - 0.6 \right)^2 + \sum_{j=1}^N \frac{1}{2} h \left\{ L_E \left(t_j, \hat{x}_j, \hat{u}_{0j}, \hat{u}_{1j}, \hat{v}_j, \hat{p}_j \right) + L_E \left(t_{j-1}, \hat{x}_{j-1}, \hat{u}_{0j}, \hat{u}_{1j}, \hat{v}_j, \hat{p}_j \right) \right\} \quad (5.2)$$

over the controls $(\hat{u}_j, \hat{v}_j) \in \Omega \times [0, 1]$, subject to equation 5.1 and any other equality constraints represented as $h(\hat{x}_{j-1}, \hat{x}_j, \hat{u}_j, \hat{v}_j, \hat{p}_j) = 0$. Here $L_E(\cdot)$ is the integrand of equation 3.4 properly discretized and \hat{p}_j represents the various power flows in the model at the midpoint.

5.2 Model Predictive Control

The MPC solution strategy in this study uses a moving four second (receding horizon) window with the control applied over 1 sec sub-intervals. In particular the NLP of the above subsection is solved over a four second window $[t_j, t_{j+1}, t_{j+2}, t_{j+3}, t_{j+4}]$ instead of the entire driving cycle. The resulting control at each iteration is applied only over the first second of the actual time window, i.e., over $[t_j, t_{j+1}]$ to the system model. The system model is then simulated over $[t_j, t_{j+1}]$ to obtain the updated state at t_{j+1} .

Of course as we approach t_f , the window shrinks appropriately. Finally for the MPC strategy the coefficient penalizing the deviation from nominal SOC, $C_{bat,j}$ is

$$C_{bat,j} = (t_{f,j} / t_f) C_{bat} \quad (5.4)$$

where $t_{f,j}$ is the final time of each MPC iteration.

6. Results: Optimal and MPC Tracking of a Sawtooth Velocity Profile

In this study, the vehicle must track a sawtooth driving profile for 40 sec on a flat road, whose rates of acceleration/deceleration and desired maximum velocity test the limits of performance of the vehicle drive train. The tradeoff among the velocity tracking error, power usages/losses, and the deviation of the SOC from nominal at the final time are explored, by choosing appropriate values of the coefficients in the PI. The vehicle's weight is set at 1890 kg similar to the hybrid SUV weights of the Ford Escape (1720 kg) or the Toyota Highlander (1850 kg).

This study compares the performances of the hybrid optimal controller (case 1) that is optimized over the entire driving cycle against an MPC version (case 2). The coefficients of the PI of equation 3.2 are $C_V = 10$,

$C_{ICE} = 10^{-3}$, $C_{FR} = 10^{-4}$, and $C_{bat,N} = 10^5$. The PI cost for the overall optimal control, 223, is smaller than the 248.5 cost for MPC, with respective fuel economies of 25.1 mpg versus 25.6 mpg for the MPC. This is primarily due to the fact that MPC deviation from nominal SOC is not significantly penalized until the end of the driving cycle as will be discussed.

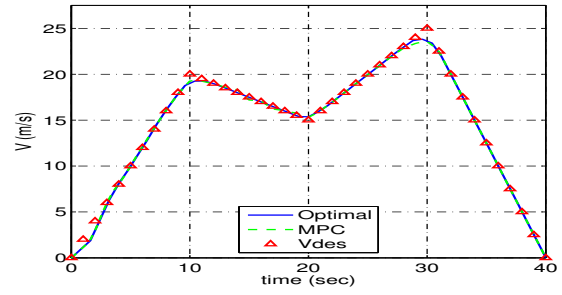


Fig. 6.1 Velocity tracking performance: (a) case 1 overall optimal hybrid control; (b) suboptimal results for MPC.

Fig. 6.1 shows relatively good velocity tracking performance for cases 1 (solid blue) and 2 (dashed green/MPC). Initially neither profile tracks perfectly although both the ED, and the ICE provide power at their maximum capacities. Also, in case 2 the vehicle velocity misses the reference peaks at 10 and 30 sec slightly more than in case 1.

Figure 6.2 illustrates that in both cases the vehicle operates in mode-0 during the first 10 sec, and in mode-1 during the last 10 sec. Between 10 and 20 sec, the vehicle operates in the generating mode less often for MPC (green dashed) because of a relatively lower penalty (coefficient) on the deviation from nominal SOC.

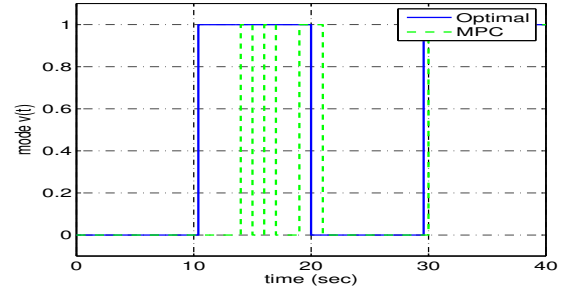


Fig. 6.2 Modes of operation: (a) case 1 (solid blue); and (b) case 2 (green dashed).

Figure 6.3 depicts the battery normalized energy (SOC) profiles. Case 1 shows consistency with the mode of operation and returns to the vicinity of the 60% nominal level at the end of the cycle. In case 2 (MPC/green dashed) SOC deviation is only mildly penalized allowing lower levels than in case 1 during the first half cycle. In the second half of the driving cycle, the vehicle draws less power from the battery in case 2 consistent with an increasing penalty on the deviation from nominal SOC.

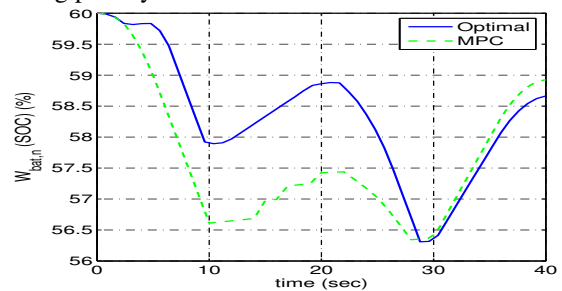


Fig. 6.3 Battery normalized energy (SOC): solid blue for case 1 and dashed green for case 2.

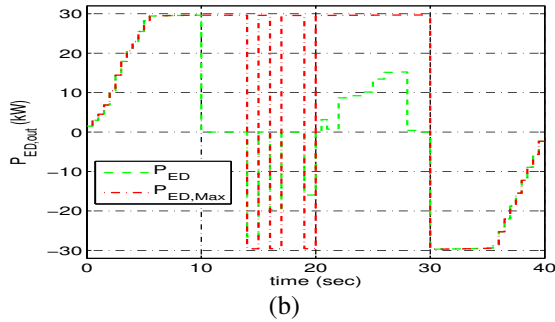
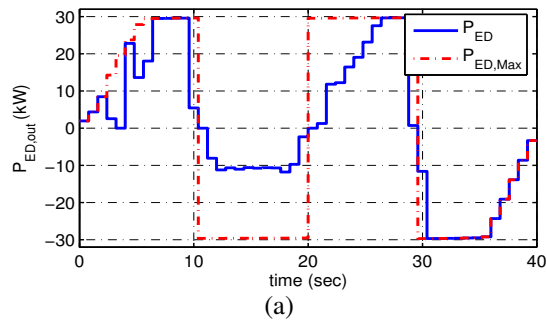


Fig. 6.4 ED output power profiles: (a) case 1 and (b) case 2

Figure 6.4 shows ED power for cases 1 and 2. For case 2, during the first 10 s the ED provides more propelling power than case 1, consistent with the above SOC profiles and the penalty coefficient of equation 5.4. Between 20 and 30 sec, the ED provides less propelling power so as not to further increase the penalty in the PI on deviation from nominal SOC as the dashed green curve is lower than the solid blue in this time frame. During the last 10 sec, the ED operates as a generator in both cases using regenerative braking power to recharge the battery and bring the SOC closer to its nominal level.

As per Figure 6.5, in both cases, the ICE is off at startup (propelling from ED alone) due to the closed-loop local ICE control constraint until a minimum operating speed of 800 RPM is reached. At about 1.2 s, in both cases, the ICE is activated to provide power slightly below the maximum level due to the built-in power train lag of 0.3 sec. In case 2, the vehicle draws less power from the ICE during the first half of the driving cycle than case 1 as shown in Fig 6.5b due to relatively lower cost on the propelling power from the ED, yielding a better fuel economy of 25.6 mpg, relative to 25.1 mpg in case 1.

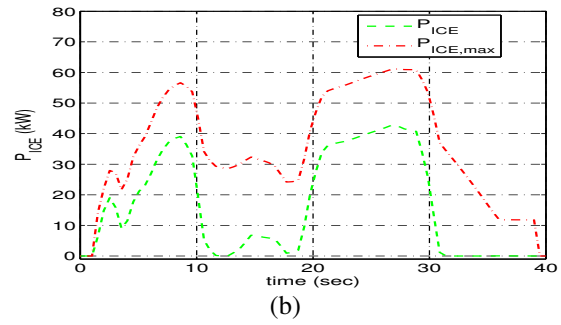
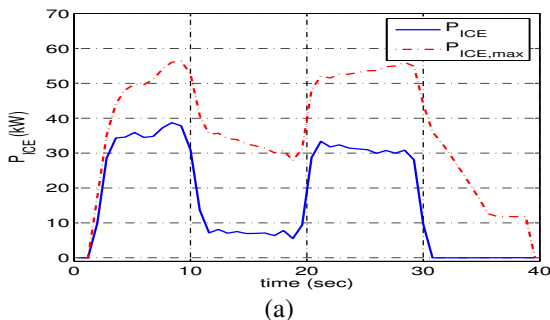


Fig. 6.5 ICE power: case 1 (solid blue); case 2 (dashed green).

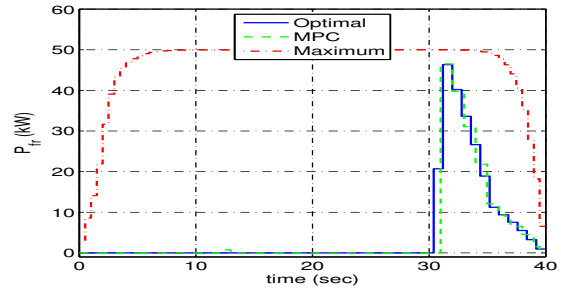


Fig. 6.6 Frictional-braking power losses: case 1 (solid blue) and case 2 (dashed green).

When the propelling power from the ED becomes more expensive in the second half of the driving cycle, the vehicle draws less power from the ED in case 2. In both cases, the ICE is shut off during the last 10 s as the vehicle slows and kinetic energy is channeled to the battery or is expended in frictional braking as shown in Figure 6.6. Indeed, frictional braking is virtually identical in both cases and is only used during the last 10 seconds of the driving profile as one would expect.

It is noted that the coefficients in the PI are selected to emphasize the velocity tracking error more than the fuel economy and the penalty on the deviation of the final SOC from the nominal level. The optimal trajectory in case 1 attains lower cost than that in case 2 despite slightly worse results on fuel economy and final SOC. If desired, one can obtain better fuel economy and closer final SOC by increasing penalty on fuel economy and final SOC deviation, at the expense of an increase in tracking error.

7. REFERENCES

- Anatone, M., Cipollone, R., and Sciarretta, A. (2005). Control-Oriented Modeling and Fuel Optimal Control of a Series Hybrid Bus. SAE 2005-01-1163.
- Bemporad, A., and Morari, M. (1999). Control of systems integrating logic, dynamics and constraints. *Automatica*, 35, pp. 407–427.
- Bengea, S. C. and DeCarlo, R. A. (2005). Optimal control of switching systems. *Automatica* 41(1), pp. 11-27.
- Bodson, M., Chiasson, J. N., and Novotnak, R.T. (1995). A Systematic approach to selecting flux references for torque maximization in induction motors. *IEEE Trans. Contr. Syst. Technol.*, 3(4), pp. 388-97.

- Brahma, A., Y. Guezennec, and G. Rizzoni (2000). Dynamic optimization of mechanical/electrical power flow in parallel hybrid electric vehicles. Proc. the 5th AVEC Int. Sym. on Advanced Vehicle Control, Ann Arbor, MI.
- Camacho E. F., and Bordons C. (2004). Model Predictive Control, 2nd Edition. Springer.
- Diop, D., Ait-Amirat, Y., Kauffmann, J. M., and El Kadri, K. (2002). Power management of a series hybrid electric vehicle. IEEE Veh. Tech. Conf, Birmingham, AL, pp. 2109-18.
- Floudas C.A. (1995). Nonlinear and Mixed Integer Optimization: Fundamentals and Applications. Oxford University Press, New York.
- Foley, D. C., Sadegh, N., Barth, E. J., and Vachtsevanos, G. J. (2001). Model identification and backstepping control of a continuously variable transmission system. Proc. of 2001 ACC, pp. 4591-6.
- Gill, P., Murray, W. and Wright, M. (1981). Practical Optimization. Academic Press.
- Giua, A., Seatzu, C., and Van Der Mee, C. (2001). Optimal control of switched autonomous linear systems. Proc. of CDC., Orlando, FL, pp. 2472-7.
- Gregory, J. and C. Lin (1992). Constrained Optimization in the Calculus of Variations and Optimal Control Theory. Van Nostrand Reinhold, New York.
- Hedlund, S., and Rantzer, A. (1999). Optimal control for hybrid systems. Proc. of CDC., Phoenix, AR, pp. 3972-7.
- Hopka, M., Brahma, A., Dilmi, S., Ercole, G., Hubert, C., Huseman, S., Kim, H., Paganelli, G., Tateno, M., Guezennec, Y., Rizzoni, G., and Washington, G. (2000). The 2000 Ohio State University Futuretruck. SAE SP-1617.
- M. Koot, Kessels, J. T. B. A., de Jager, B., Heemels, W. P. M. H., van den Bosch, P. P. J, and Steinbuch, M. (2005). Energy management strategies for vehicular electric power systems. IEEE Trans. Veh. Technol., 54(3), pp. 771-82.
- Lin, C. C., Peng, H., Grizzle, J. W., and Kang, J. M. (2003). Power management strategy for a parallel hybrid electric truck. IEEE Trans. Contr. Syst. Technol., 11(6), pp. 839-49.
- Nemhauser, G.L. and Wolsey, L.A. (1988). Integer and Combinatorial Optimization, John Wiley, New York.
- Neuman, C. P. and Sen, A. (1973). A suboptimal control algorithm for constrained problems using cubic splines. Automatica, vol. 9, pp. 601-13.
- G. Paganelli, M. Tateno, A. Brahma, G. Rizzoni, and Y. Guezennec, "Control development for a hybrid-electric sport-utility vehicle: Strategy, implementation and field test results," Arlington, VA, 2001.
- Powell, B. K., Bailey, K. E. and Cikanek, S. R. (1998). Dynamic modeling and control of hybrid electric vehicle powertrain systems. IEEE Contr. Syst. Mag., 18(5), pp. 17-33.
- Pytlak, R. and Vinter, R. B. (1995). Second-order method for optimal control problems with state constraints and piecewise-constant controls. Proc. IEEE CDC, New Orleans, LA.
- Rahman, Z., Butler, K. L., and Ehsani, M. (2000). A Comparison study between two parallel hybrid control concepts. SAE Technical Papers 2000-01-0994.
- Rizzoni, G., Guzzella, L., and Baumann, B. (1999). Unified modeling of hybrid electric vehicle drivetrains. IEEE/ASME Trans. Mechatron., 4(3), pp. 246-57.
- Pisu, P. and Rizzoni, G. (2007). A comparative study of supervisory control strategies for hybrid electric vehicles. IEEE Trans. Contr. Syst. Technol., 15(3), pp. 506-18.
- P. Riedinger, Zanne, C. and Kratz, F. (1999). Time optimal control of hybrid systems. Proc. ACC., San Diego, CA.
- Setlur, P., Wagner, J. R., Dawson, D. M., and Samuels, B. (2003). Nonlinear control of a continuously variable transmission (CVT). IEEE Trans. Contr. Syst. Technol., 11(1), pp. 101-8.
- Sussmann, H. (1999). A maximum principle for hybrid optimal control problems. Proc. of CDC, Phoenix, AR, pp. 425-30.
- Uthaichana, K., Bengea, S., and DeCarlo, R. A. (2005). Suboptimal Supervisory Level Power Flow Control of a Hybrid Electric Vehicle. Proc. 16th IFAC World Congress, Prague.
- Uthaichana, K. (2006). Modeling and control of a parallel hybrid electric vehicle, Ph.D. Dissertation, School of Electrical and Computer Engineering, Purdue University, West Lafayette, IN, December.
- Waltermann, P. (1996) Modelling and control of the longitudinal and lateral dynamics of a series hybrid vehicle. Proc. IEEE Intl. Conf. on Control App., Dearborn, MI, pp. 191-8.
- Wasynczuk, O., Sudhoff, S. D., Corzine, K. A., Tichenor, J. L., Krause, P. C., Hansen, I. G., and Taylor, L. M. (1998). A maximum torque per ampere control strategy for induction motor drives. IEEE Trans. Energy Convers. 13(2), pp. 163-9.
- Wei, S., Uthaichana, K., Zefran, M., DeCarlo, R. A. and Bengea S. (2007). Applications of Numerical Optimal Control to Nonlinear Hybrid Systems. Nonlinear Analysis: Hybrid Systems and Applications. 1(2), pp. 264-79.
- Won, J.-S., Langari, R. and Ehsani, M. (2005). An energy management and charge sustaining strategy for a parallel hybrid vehicle with CVT. IEEE Trans. Contr. Syst. Technol., 13(2), pp. 313-20.
- Zefran, M. (1996). Continuous Methods for Motion Planning. Ph.D Thesis, University of Pennsylvania, Philadelphia.